ORGANOMETALLICS

Article

pubs.acs.org/Organometallics

Spin Trapping of Carbon-Centered Ferrocenyl Radicals with Nitrosobenzene

Andreas Neidlinger,[†] Torben Kienz,[†] and Katja Heinze*

Institute of Inorganic and Analytical Chemistry, Johannes Gutenberg-University, Duesbergweg 10-14, D-55128 Mainz, Germany

Supporting Information

ABSTRACT: In contrast to metal centered 17 valence electron radicals, such as $[Mn(CO)_5]^\bullet$, ferrocenium ions $[Fe(C_5H_5)_2]^+$ ($\mathbf{1}^+$), $[Fe(C_5Me_5)_2]^+$ ($\mathbf{2}^+$), $[Fe(C_5H_5)(C_5H_4Et)]^+$ ($\mathbf{3}^+$), $[Fe(C_5H_5)$-$(C_5H_4NHC(O)Me)]^+$ ($\mathbf{4}^+$), and $[Fe(C_5H_5)(C_5H_4NHC(S)Me)]^+$ ($\mathbf{5}^+$) do not add to nitrosobenzene PhNO to give metal-coordinated stable nitroxyl radicals. In the presence of the strong and oxidatively stable phosphazene base *tert*-butylimino-tris(dimethylamino)-phosphorane, the quite acidic ferrocenium ions $\mathbf{1}^+$–$\mathbf{5}^+$ are deprotonated to give a pool of transient and persistent radicals with different deprotonation sites $[\mathbf{1}\text{–}\mathbf{H}^x]^\bullet$–$[\mathbf{5}\text{–}\mathbf{H}^x]^\bullet$. One rather persistent iron-centered radical $[\mathbf{4}\text{–}\mathbf{H}^N]^\bullet$, deprotonated at the nitrogen atom, has been detected by rapid-freeze EPR spectroscopy at 77 K. This iron-centered radical $[\mathbf{4}\text{–}\mathbf{H}^N]^\bullet$ is also inert toward PhNO. The transient carbon-centered radicals $[\mathbf{1}\text{–}\mathbf{H}^x]^\bullet$–$[\mathbf{5}\text{–}\mathbf{H}^x]^\bullet$ appear to rapidly abstract hydrogen atoms from the adjacent base or the solvent to regenerate the corresponding ferrocenes **1**–**5**. These transient radicals are only present in trace amounts (<1%). However, some of the transient carbon-centered radicals in the radical pool can be trapped by 1–1.2 equiv of PhNO, even at room temperature. The corresponding resulting stable nitroxyl radicals $[\mathbf{6}]^\bullet$–$[\mathbf{10}]^\bullet$ were studied by EPR spectroscopy at room temperature and at 77 K. The hyperfine coupling pattern to protons close to the spin center allows one to assign the site of PhNO attack in radicals $[\mathbf{6}]^\bullet$–$[\mathbf{10}]^\bullet$, namely, at the C_5H_5 ring in $[\mathbf{6}]^\bullet$, $[\mathbf{9}^{Cp}]^\bullet$, and $[\mathbf{10}^{Cp}]^\bullet$, at a methyl group in $[\mathbf{7}]^\bullet$, and at the methylene group in $[\mathbf{8}^1]^\bullet$. These studies give a deeper insight into the stability and reactivity of radicals derived from ferrocene derivatives which might also be relevant for the biological activity of high-potent antitumor and antimalaria ferrocene-based drugs and prodrugs such as ferrocifen or ferroquine.

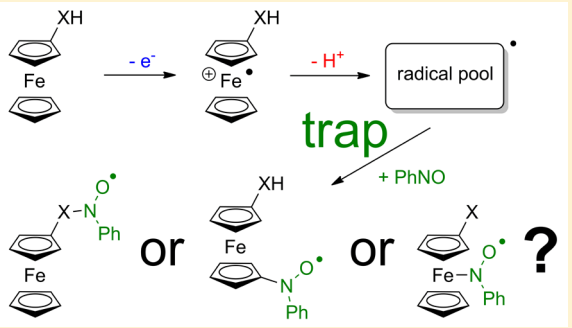

INTRODUCTION

Ferrocene and its derivatives have been found useful for a variety of applications in fundamental research, especially electron transfer, in biology and catalysis, as well as in material and pharmaceutical science.[1−5] While many of these applications rely on the reversible oxidation chemistry of the ferrocenyl moiety, investigation of the reactivity and possible degradation pathways of the resulting ferrocenium cations is worthwhile.

For instance, ferrocene itself displays no antitumor activity, while ferrocenium derivatives show in vitro cytotoxicity due to oxidative damage of DNA.[6] This has been further exploited using amino ferrocene based selective prodrugs **A** by Mohkir et al. (Scheme 1). In tumor cells, ferrocenes **A** are oxidized to the corresponding ferrocenium ions $\mathbf{A}^+$. The ferrocenium cations $\mathbf{A}^+$, as well as their degradation products, iron(II) ions, appear to catalyze the generation of reactive oxygen species. This increases the oxidative stress in cancer cells and finally leads to apoptosis.[7,8] This concept has been further explored with a variety of amino ferrocene and diamino ferrocene based prodrugs (**B**; Scheme 1a). The degradation products of $\mathbf{B}/\mathbf{B}^+$ again act as catalysts for generating reactive oxygen species.[9] In fact, first in vivo experiments show promising results for further pharmaceutical applications.[10]

The effectiveness of the antimalarial drug chloroquine **C** has been drastically improved by incorporation of a ferrocenyl moiety giving the potent drug ferroquine **D** (Scheme 1b). This adds the generation of reactive oxygen species as a further mode of action to the drug and takes effect in all stages of the life cycle of the parasites, thus inhibiting merozoites reinvasion.[11−13]

While the generation of reactive oxygen species is a valuable mechanism for amino ferrocene based prodrugs **A** and **B** and ferroquine **D**, other antitumor agents appear to follow a different mode of action. The ferrocene derivatives of tamoxifen **E**, ferrocifen **F**, and ferrociphenol **G** (Scheme 1c) show high levels of cytotoxicity against breast cancer cells. Ferrocifen **F** is even more cytotoxic than *cis*-platin.[14−18] Both ferrocifen **F** and hydroxyferrocifen **G** cause less oxidative stress compared to that of tamoxifen **E**.[19,20] Yet, in cells treated with ferrocifen derivatives a higher rate of senescence has been found. As this is unlikely to be related to oxidative stress, a further mode of action is assumed showing the versatility of ferrocenium ions. Indeed, carbon-centered radicals have been proposed to be generated after oxidation and deprotonation of ferrocifens **F**.[16]

Received: September 13, 2015
Published: October 27, 2015

DOI: 10.1021/acs.organomet.5b00778
Organometallics 2015, 34, 5310−5320

Scheme 1. (a) Aminoferrocene Based Prodrugs A, B; (b) Chloroquine C and Ferroquine D; (c) Tamoxifen E, Ferrocifen F, and Ferrociphenol G

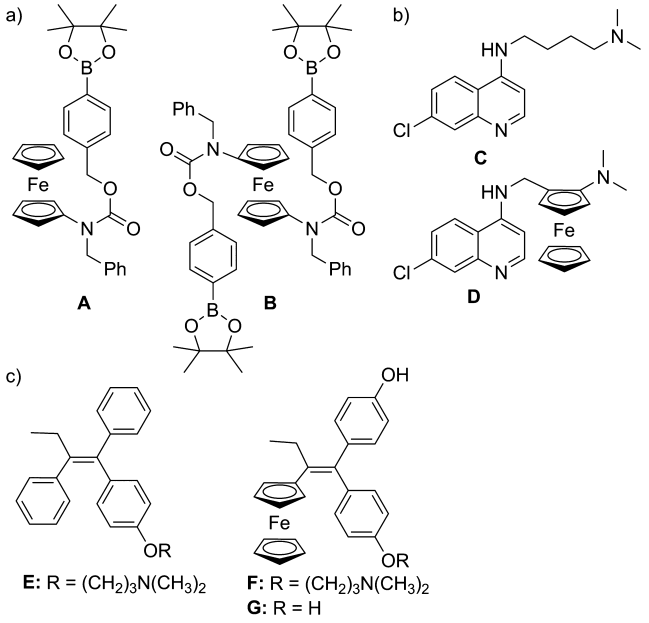

Various experiments have been reported which focus on the ability of ferrocene to form radicals itself. First hints to the existence of ferrocenyl radicals were obtained by photo- and thermolysis of ferrocenyl azide by Sutherland et al.[21] γ-Irradiation of methylferrocene led to the ferrocenyl methyl-radical.[22] Later, it was found that ferrocenyl substituted radicals are stabilized due to spin delocalization to the iron atom.[23] This can even be exploited to generate polymetallocenylenes[24] or in stereoselective pinacol coupling reactions.[25]

The radical reactivity of ferrocenium ions has been demonstrated by the oxidation of ferrocenophanes with silver salts in the presence of sodium methoxide. As reported by Hisatome et al., this procedure results in the intermediate formation of a carbon-centered radical in the aliphatic bridge (Scheme 2a). Ferrocenylmethylium cations, as shown by Ashkenazi and Cais, react as biradicals with nitrosobenzene PhNO as spin trap (Scheme 2b).[26]

Obviously, spin trapping is a valuable tool for the investigation of transient radicals. Indeed, various manganese centered 17 valence electron radicals prepared by homolysis of carbonyl complexes could be spin trapped with nitrosodurene as spin trapping agent by Hudson and Lappert[27] as well as with 2,4,6-tri(*tert*-butyl)nitrosobenzene by Simpson et al.[28] and with the aid of nitroso-*tert*-butane by Benner and Balch.[29] Later on, Re, Co, Fe, and Mo centered 17 valence electron radicals could be trapped with 2,3,5,6-tetramethyl-1-nitrosobenzene as spin trapping agent and identified by EPR spectroscopy (Scheme 2c).[30]

With the versatile and not yet fully understood reaction pathways of ferrocenium ions in mind, we were interested to generate and trap radical species of different ferrocenium ions under neutral and strongly basic conditions using the spin trapping technique. The starting iron(III) complexes ferrocenium ($\mathbf{1}^+$), decamethylferrocenium ($\mathbf{2}^+$), ethylferrocenium ($\mathbf{3}^+$), *N*-acetylaminoferrocenium ($\mathbf{4}^+$), and *N*-thioacetylaminoferrocenium ($\mathbf{5}^+$) were prepared by oxidation of the corresponding ferrocenes **1**−**5** with silver hexafluoroantimonate. Spin trapping

Scheme 2. (a) Oxidation and Deprotonation of [4]ferrocenophane; (b) Spin Trapping of a Ferrocenylmethylium Ion with Nitrosobenzene; and (c) Spin Trapping of Metal Centered 17 Valence Electron Radicals

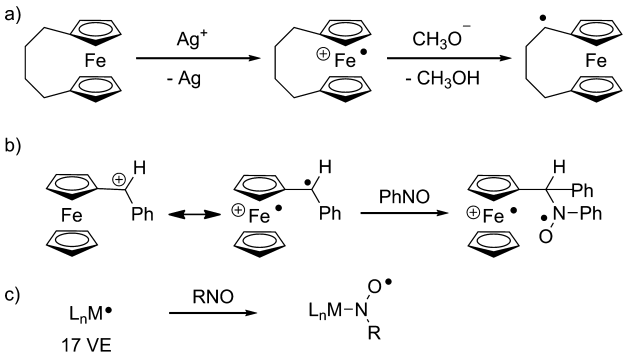

L_nM = $Mn(CO)_5$, $Re(CO)_5$, $Co(CO)_3[P(OEt)_3]$, $Fe(CO)_2Cp$, $Mo(CO)_3Cp$,...
R = C_6H_5, $C_6H_2(C(CH_3)_3)_3$, $C_6(CH_3)_5$, $C_6H(CH_3)_4$, $C(CH_3)_3$

of radicals was attempted with nitrosobenzene (PhNO) in the absence and presence of the strong, non-nucleophilic, non-coordinating, and oxidatively stable phosphazene base $P_1{}^tBu$ (*tert*-butylimino-tris(dimethylamino)phosphorane (Scheme 3). In the presence of $P_1{}^tBu$, $\mathbf{1}^+$−$\mathbf{5}^+$ are expected to yield the corresponding radicals or radical pools [**1**−**H**]•−[**5**−**H**]•. In order to address the question as to whether radicals are formed at

Scheme 3. Spin Trapping Reactions of Ferrocenium Derivatives in the Absence and Presence of $P_1{}^tBu$ for (a) $\mathbf{1}^+$, (b) $\mathbf{2}^+$, (c) $\mathbf{3}^+$, and (d) $\mathbf{4}^+$ and $\mathbf{5}^+$ Investigated in This Study[a]

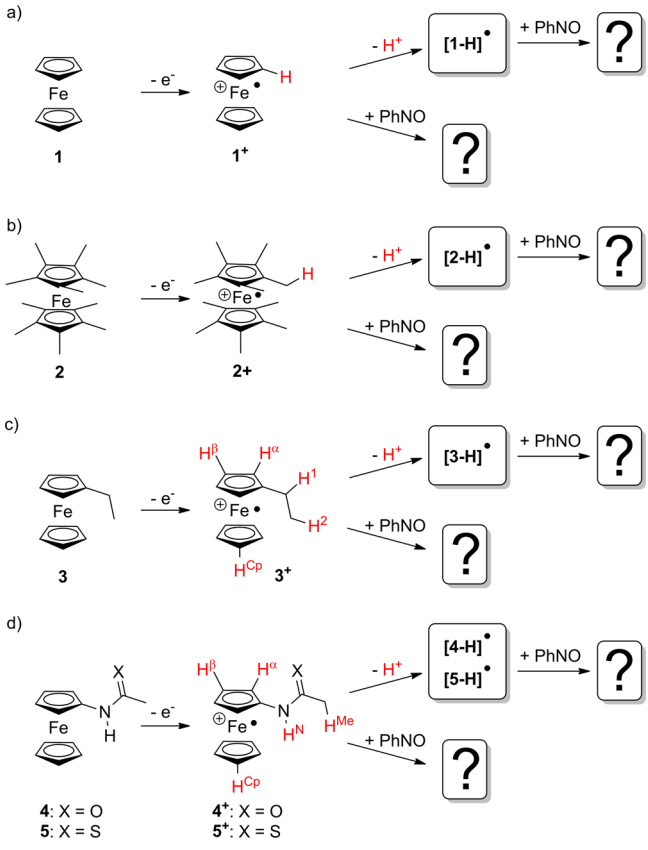

[a]Relevant atom numbering is given. Possible acidic hydrogen atoms are marked in red.

DOI: 10.1021/acs.organomet.5b00778
Organometallics 2015, 34, 5310−5320

all and to identify the site of the generated radicals (carbon, iron, nitrogen centered), the conceivable spin trapped nitroxide radical adducts of $\mathbf{1}^+-\mathbf{5}^+$ and $[\mathbf{1}-\mathbf{H}]^\bullet-[\mathbf{5}-\mathbf{H}]^\bullet$ were probed by EPR spectroscopy (Scheme 3).

While ferrocenyl nitroxide radicals have been prepared via autoxidation of ferrocenyl hydrazine and investigated by EPR spectroscopy by Forrester and Hepburn, the present approach offers a different and more general access to ferrocenyl nitroxyl radicals.[31a] Elschenbroich has reported the electrochemical generation and EPR spectroscopic study of isoelectronic radical anions of ferrocenyl arylketones.[31b] Similarly, ferrocenoylsilanes have been reduced to the corresponding radical anions by Grignard reagents.[31c]

Reactions of ferrocenium $\mathbf{1}^+$ with nitrogen bases (pyrazolide, 3,5-dimethyl pyrazolide, imidazolide, and benzotriazolide) have been reported in the literature.[32] Yet, these bases are oxidized by the ferrocenium cation $\mathbf{1}^+$ to the corresponding azolide radicals while $\mathbf{1}^+$ is reduced to **1**. The azolide radicals are suggested to attack $\mathbf{1}^+$ to give *N*-ferrocenyl azoles after proton loss (Scheme 4). No ferrocenyl radicals were reported. Clearly, such a reactivity is not expected with the base $P_1{}^tBu$ employed in this study.

Scheme 4. Suggested Mechanism of the Formation of *N*-Ferrocenylpyrazole from Ferrocenium Radical Cations and Pyrazolide Anions[32]

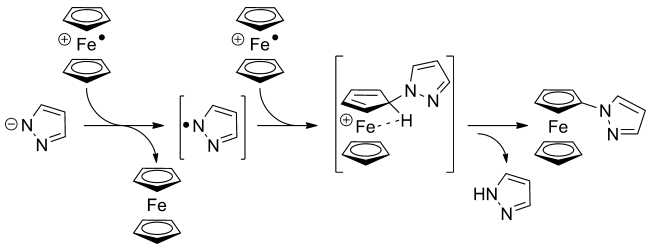

RESULTS AND DISCUSSION

Spin Trapping of Ferrocenium Ions. The oxidations of ferrocenes **1**−**5** to their respective cations $\mathbf{1}^+-\mathbf{5}^+$ (Scheme 3) are performed in CH_2Cl_2 under inert conditions using one equivalent of silver hexafluoroantimonate $AgSbF_6$ as oxidant as its oxidation potential [$E_{1/2}(CH_2Cl_2)$ = 650 mV vs FcH/FcH$^+$][33a] is sufficient for this purpose [$E_{1/2}(CH_2Cl_2)$ = 0,−480,−55,−50,−20 mV for **1**−**5**, respectively].[33] Furthermore, the coproduct silver is easily removed by filtration.

The presence of 1−1.2 equiv of PhNO does not influence the EPR spectra of the ferrocenium ions. Indeed, $\mathbf{1}^+$ is EPR silent both at 298 K and at 77 K as its EPR spectrum has been observed only below 20 K due to fast spin−lattice relaxation.[34] No EPR resonances are observed in the presence of PhNO as well. Obviously, the iron-centered 17 valence electron radical $\mathbf{1}^+$ does not add to PhNO to give the conceivable nitroxide adduct $[\mathbf{1\text{-}PhNO}]^+$, in contrast to what has been reported for $[Mn(CO)_5]^\bullet$ radicals for example (Scheme 2c). DFT calculations for $\mathbf{1}^+$, PhNO, and $[\mathbf{1\text{-}PhNO}]^+$ account for this lack of reactivity as the formation of $[\mathbf{1\text{-}PhNO}]^+$ is endergonic by 49 kJ mol^{-1} (Supporting Information, Figure S1).

Similarly, $\mathbf{4}^+$ gives a nearly axial EPR resonance at 77 K in frozen solution[35] which remains unchanged in the presence of PhNO. At room temperature, $\mathbf{4}^+$ and the $\mathbf{4}^+$/PhNO mixture are EPR-silent. Obviously, iron-centered ferrocenium radical ions are unable to react with PhNO to give the nitroxyl radicals. This behavior contrasts the reactivity of other organometallic 17 valence electron complexes (Scheme 2c).[27−30]

Spin Trapping of Ferrocenium Ions in the Presence of a Base. The ferrocenium ions $\mathbf{1}^+-\mathbf{5}^+$ were treated with one equivalent of the non-nucleophilic and noncoordinating phosphazene base $P_1{}^tBu$ (*tert*-butylimino-tris(dimethylamino)-phosphorane, (pK_a (MeCN) = 26.98)[36] as a proton acceptor. To ensure that the ferrocenium salts $\mathbf{1}^+-\mathbf{5}^+$ are unable to oxidize the employed $P_1{}^tBu$ base, its redox potential has been determined by cyclic voltammetry. Indeed, $P_1{}^tBu$ is irreversibly oxidized at E_p = 400 mV vs FcH/FcH$^+$ ($[^nBu_4N][B(C_6F_5)_4]/CH_2Cl_2$), significantly higher than the redox potentials of the $\mathbf{1}/\mathbf{1}^+-\mathbf{5}/\mathbf{5}^+$ redox couples (Figure S2). A mechanistic scenario as shown in Scheme 4 for heterocyclic nitrogen bases is possible in principle due to the irreversible nature of the $P_1{}^tBu/P_1{}^tBu^+$ oxidation, although it is not very likely. Hence, a simple deprotonation of $\mathbf{1}^+-\mathbf{5}^+$ to give the radicals and radical pools $[\mathbf{1}-\mathbf{H}]^\bullet-[\mathbf{5}-\mathbf{H}]^\bullet$ should be achieved (Scheme 3). As illustrated in Scheme 3, deprotonation of $\mathbf{1}^+$ and $\mathbf{2}^+$ should yield the radicals $[\mathbf{1}-\mathbf{H}]^\bullet$ and $[\mathbf{2}-\mathbf{H}]^\bullet$, respectively. As $\mathbf{3}^+$, $\mathbf{4}^+$, and $\mathbf{5}^+$ possess five chemically different protons, which might be abstracted, radical pools consisting of up to five radical species might be present. The different radicals will be designated by the location of the abstracted proton as $[\mathbf{3}-\mathbf{H}^{Cp}]^\bullet$, $[\mathbf{3}-\mathbf{H}^{\alpha}]^\bullet$, $[\mathbf{3}-\mathbf{H}^{\beta}]^\bullet$, $[\mathbf{3}-\mathbf{H}^{1}]^\bullet$, and $[\mathbf{3}-\mathbf{H}^{2}]^\bullet$ for the radical pool $[\mathbf{3}-\mathbf{H}]^\bullet$; $[\mathbf{4}-\mathbf{H}^{Cp}]^\bullet$, $[\mathbf{4}-\mathbf{H}^{\alpha}]^\bullet$, $[\mathbf{4}-\mathbf{H}^{\beta}]^\bullet$, $[\mathbf{4}-\mathbf{H}^{N}]^\bullet$, and $[\mathbf{4}-\mathbf{H}^{Me}]^\bullet$ for the radical pool $[\mathbf{4}-\mathbf{H}]^\bullet$; and $[\mathbf{5}-\mathbf{H}^{Cp}]^\bullet$, $[\mathbf{5}-\mathbf{H}^{\alpha}]^\bullet$, $[\mathbf{5}-\mathbf{H}^{\beta}]^\bullet$, $[\mathbf{5}-\mathbf{H}^{N}]^\bullet$, and $[\mathbf{5}-\mathbf{H}^{Me}]^\bullet$ for the radical pool $[\mathbf{5}-\mathbf{H}]^\bullet$ (Scheme 3). Trapping of these radicals or some of these radicals by the spin trapping technique using nitrosobenzene PhNO is attempted. We will start with the simple ferrocene and decamethylferrocene derivatives $[\mathbf{1}-\mathbf{H}]^\bullet$ and $[\mathbf{2}-\mathbf{H}]^\bullet$ and then describe the more diverse reactivity of $[\mathbf{3}-\mathbf{H}]^\bullet-[\mathbf{5}-\mathbf{H}]^\bullet$. DFT calculations were employed both for the radical species $[\mathbf{1}-\mathbf{H}]^\bullet-[\mathbf{5}-\mathbf{H}]^\bullet$ as well as for the conceivable corresponding PhNO adducts $[\mathbf{6}]^\bullet-[\mathbf{10}]^\bullet$.

For the $\mathbf{1}^+$/PhNO/$P_1{}^tBu$ mixture, an EPR triplet resonance at g_{iso} = 2.0063 with nitrogen hyperfine coupling (hfc) $A(^{14}N)$ = 11.1 G was recorded (Figure 1), similar to typical nitroxyl

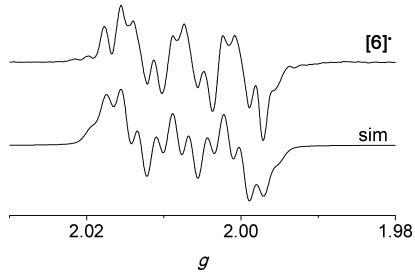

Figure 1. X-band EPR spectrum (top) and simulated spectrum (bottom) of $[\mathbf{6}]^\bullet$ (20 mM **1** in CH_2Cl_2) at the following experimental parameters: temperature = 298 K, field = 3358.98 G, sweep = 298.72 G, sweep time = 120 s, modulation = 1000 mG, and MW attenuation = 9 dB.

radicals.[37−40] Furthermore, hyperfine couplings to hydrogen nuclei of the phenyl moiety and the substituted cyclopentadienyl ring are extracted from the simulation of the EPR resonance (Table 1). H^o, H^m, and H^p denote the *ortho*, *meta*, and *para* protons of the phenyl substituent, respectively, while H^α and H^β are the *alpha* and *beta* protons of the substituted Cp ring. The observed coupling pattern allows a clear assignment to the ferrocenyl phenyl nitroxide radical $[\mathbf{6}]^\bullet$ (*N*-oxyl-*N*-phenyl-

DOI: 10.1021/acs.organomet.5b00778
Organometallics 2015, 34, 5310−5320

Table 1. EPR Parameters Obtained by the Simulation of Experimental Spectra (298 K)

radical	g_{iso}	A(14N) (G)	$A(^1H^o)$ (G) (2×)	$A(^1H^m)$ (G) (2×)	$A(^1H^p)$ (G)	$A(^1H^\alpha)$ (G)	$A(^1H^\beta)$ (G)	$A(^1H^1)$ (G)	Gauss pp line width (MHz)	Lorentz pp line width (MHz)
[**6**]•	2.0063	11.10	2.90	0.80	2.70	3.80 (2×)	0.60 (2×)		0.15	0.08
[**7**]•	2.0068	11.07	2.77	0.95	2.64			8.64 (2×)	0.02	0.015
[**8**^{1}]•	2.0072	11.16	2.77	1.00	2.65			2.10	0.035	0.065
[**9**^{Cp}]•	2.0072	10.90	2.77	0.90	2.64	1.20/1.10	0.70 (2×)		0.06	0.02
[**10**^{Cp}]•	2.0068	11.09	2.77	0.91	2.64	2.55/2.10	1.82/1.08		0.085	0.005

Table 2. EPR Parameters Obtained by the Simulation of Experimental Spectra (77 K)

radical (mixture)	$g_{1,2,3}$	$A(^{14}N)$ (G)	fraction (%)	Gauss pp line width (MHz)	Lorentz pp line width (MHz)
[**6**]•	2.0104, 2.0068, 2.0040	4.0, 4.0, 26.0		0.90	0.30
[**7**]•	2.0094, 2.0067, 2.0048	4.0, 4.0, 26.0		1.50	0.60
[**8**^{1}]•	2.0095, 2.0073, 2.0045	3.0, 3.0, 27.5		0.90	0.40
[**9**^{Cp}]	2.0105, 2.0060, 2.0045	3.5, 3.5, 28.0	17	0.30	0.40
[**4**−**H**^{N}]•	N/A[a], 1.9620, 1.9450	N/A	83	0.50	0.20
[**4**−**H**^{x}]• (x = α,β,Cp,Me)	2.0095, 2.0065, 2.0030		0.8	0.30	0.2
[**4**−**H**^{N}]•	N/A[a], 1.9650, 1.9400		99.2	0.1	0.1
[**10**^{Cp}]•	2.0105, 2.0060, 2.0020	3.5, 3.5, 28.0	5	0.60	0.60
[**11a**]•	2.3100, 2.0695, 1.9990		48	0.50	0.50
[**11b**]•	2.2250, 2.0565, 2.0095		47	0.50	0.50

[a]Too broad to be observed.

ferrocenylamine). The hfc to ^{14}N in [**6**]• is close to the observed hfc in the reported nitroxide radical [Fc-N(O)-tBu]• [$A(^{14}N)$ = 11.75 G].[31a] Some phenyl hydrogen hfc's of [**6**]• are similar to those obtained for the isoelectronic radical anion [Fc-C(O)-Ph]•−.[31b] At 77 K, a slightly anisotropic signal at $g_{av} \approx 2.0071$ with a large nitrogen hyperfine coupling of $A(^{14}N)$ = 26 G in the high field region is recorded (Table 2; Figure S4a). Hyperfine couplings to hydrogen atoms are not resolved in the frozen solution spectrum, and hence, a larger line width was applied in the simulation instead.

Obviously, the increased acidity of the positively charged ferrocenium ion **1**$^+$[35,41] allows C−H deprotonation by P_1^tBu. The initially formed *C*-deprotonated zwitterionic ferrocenium species corresponds to an electronically excited state and relaxes to the carbon centered radical [**1**−**H**]• by internal electron transfer (Figure S3a; Mulliken spin density at C 0.787; Mulliken spin density at Fe 0.212). The *C*-centered radical [**1**−**H**]• attacks the nitrogen atom of PhNO leading to the spin trapped nitroxyl radical *N*-oxyl-*N*-phenyl-ferrocenylamine [**6**]• (Figure 2a). DFT calculations revealed that the nitroxyl radical [**6**]• is lower in energy than the starting materials [**1**−**H**]• and PhNO by 208 kJ mol^{-1} (Figure S3a), explaining the facile formation of [**6**]•.

Successful deprotonation of **1**$^+$ with P_1^tBu was further evidenced by cyclic voltammetry of **1** in the absence and presence of the base using tetra(*n*-butyl)ammonium tetrakis-(pentafluorophenyl)borate ([$^nBu_4N$][$B(C_6F_5)_4$]) as weakly coordinating electrolyte.[42,43] Expectedly, ferrocene **1** shows a reversible one-electron redox process at a potential of $E_{1/2}$ = 0 V vs FcH/FcH$^+$ per definition (Figure S5a). Addition of a stoichiometric amount of P_1^tBu renders this oxidation irreversible, due to the deprotonation of **1**$^+$ to [**1**−**H**]• and follow up reactions of the highly reactive *C*-centered radical [**1**−**H**]• (Figure S5b). As the oxidation process occurs at essentially the same potential (against the $Ag/AgNO_3$ reference electrode) in the presence of P_1^tBu, deprotonation of **1** to [**1**−**H**]$^-$ by P_1^tBu prior to oxidation is unlikely. Deprotonation of ferrocene **1**, however, is achieved using alkyl lithium bases as a well-known starting point for the rich ferrocene substitution chemistry.[44−47]

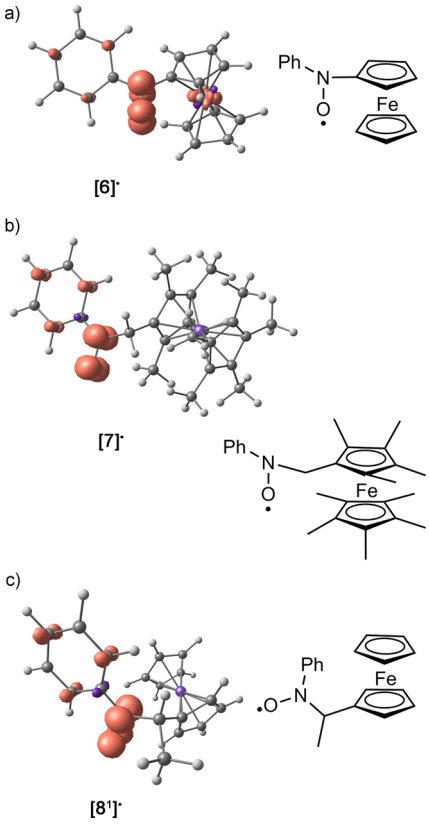

Figure 2. DFT optimized geometries with spin densities (0.01 au isosurface value) in CH_2Cl_2 continuum solvent as well as Lewis structures of nitroxide radicals (a) [**6**]•, (b) [**7**]•, and (c) [**8**^{1}]•.

Despite the lack of aromatic C−H atoms, decamethylferrocenium **2**$^+$ reacts with PhNO as well in the presence of P_1^tBu (Scheme 3b). Obviously, the methyl groups become sufficiently acidic upon oxidation of **2** to **2**$^+$ due to the increased electron deficiency. Hence, the *C*-centered radical [**2**−**H**]• is generated

DOI: 10.1021/acs.organomet.5b00778
Organometallics 2015, 34, 5310−5320

from 2^+ by deprotonation of a CH_3 group (Figure S3b, Mulliken spin density at C 0.650; Mulliken spin density at Fe 0.513). Similar to $[1-H]^\bullet$, $[2-H]^\bullet$ is trapped by PhNO resulting in the formation of the nitroxide radical $[7]^\bullet$ 1-[(*N*-oxyl-*N*-phenylamino)methyl]-1′,2,2′,3,3′,4,4′,5,5′-nonamethylferrocene (Figure 2b). The driving force for the formation of $[7]^\bullet$ from the starting materials $[2-H]^\bullet$ and PhNO (Figure S3b) is calculated as 80 kJ mol^{-1} by DFT methods. At 298 K, $[7]^\bullet$ gives an EPR resonance with parameters summarized in Table 1 (Figure 3). The nitrogen and hydrogen hyperfine couplings for

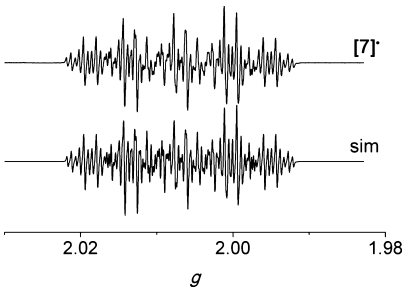

Figure 3. X-band EPR spectrum (top) and simulated spectrum (bottom) of $[7]^\bullet$ (25 mM **2** in CH_2Cl_2) at the following experimental parameters: temperature = 298 K, field = 3346.20 G, sweep = 94.79 G, sweep time = 90 s, modulation = 250 mG, and MW attenuation = 5 dB.

the PhNO moiety of $[7]^\bullet$ are very similar to those of $[6]^\bullet$. The two large hydrogen hyperfine couplings of $[7]^\bullet$ ($A(^1H)$ = 8.64 G), obtained by simulation, are assigned to the protons of the methylene group. The large hfc's nicely fit to the reported hfc's for the ferrocenylmethyl radical prepared from methylferrocene by γ-irradiation ($A(^1H)$ = 14.71 G).[22] At 77 K in frozen solution, the nitroxide radical $[7]^\bullet$ displays a slightly anisotropic resonance similar to that of $[6]^\bullet$ (Figure S4b) with one large nitrogen hyperfine coupling component (Table 2). Again, hydrogen hyperfine couplings are not resolved under these conditions.

In contrast to **1** and **2**, ethylferrocene **3** has five chemically different protons resulting in five conceivable *C*-centered radicals $[3-H^{Cp}]^\bullet$, $[3-H^{\alpha}]^\bullet$, $[3-H^{\beta}]^\bullet$, $[3-H^{1}]^\bullet$, and $[3-H^{2}]^\bullet$ (Scheme 3c). Consequently, five distinct nitroxyl radicals can in principle be obtained from this radical pool by reaction with PhNO, namely, $[8^{Cp}]^\bullet$, $[8^{\alpha}]^\bullet$, $[8^{\beta}]^\bullet$, $[8^{1}]^\bullet$, and $[8^{2}]^\bullet$. Despite the possible mixture of products, the room temperature EPR spectrum of $[8]^\bullet$ is well resolved, suggesting the presence of only a single nitroxide radical (Figure 4). The EPR pattern of $[8]^\bullet$ is well reproduced by assuming the typical ^{14}N and ^1H hfc's

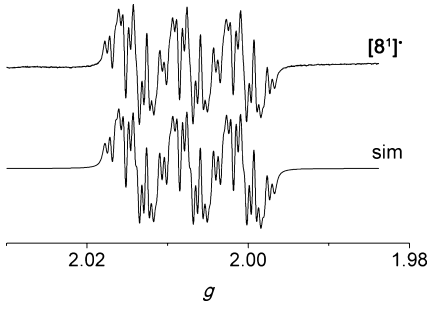

Figure 4. X-band EPR spectrum (top) and simulated spectrum (bottom) of $[8^1]^\bullet$ (25 mM **3** in CH_2Cl_2) at the following experimental parameters: temperature = 298 K, field = 3346.20 G, sweep = 94.79 G, sweep time = 90 s, modulation = 250 mG, and MW attenuation = 0 dB.

of the PhNO unit in addition to a further hfc to a single hydrogen atom (Table 1). This perfectly fits to the $[8^1]^\bullet$ nitroxide radical with the PhNO substituent attached to the C^1 atom of the ethyl substituent. For all other nitroxide radicals $[8^{Cp}]^\bullet$, $[8^{\alpha}]^\bullet$, $[8^{\beta}]^\bullet$, and $[8^2]^\bullet$, more than one chemically different hydrogen atom would have been expected to display hfc's. At 77 K, a similar spectrum as that for $[6]^\bullet$ is recorded for $[8^1]^\bullet$ (Table 2; Figure S4c).

The presence of only a single product $[8^1]^\bullet$ derived from $[3-H^1]^\bullet$ is straightforwardly explained by the pronounced stability of the secondary *C*-centered radical $[3-H^1]^\bullet$ by more than 60 kJ mol^{-1} with respect to all other radicals $[3-H^{Cp}]^\bullet$, $[3-H^{\alpha}]^\bullet$, $[3-H^{\beta}]^\bullet$, and $[3-H^2]^\bullet$ according to DFT calculations (Figure S6, Mulliken spin density at C^1 0.757; Mulliken spin density at Fe 0.341). However, all five conceivable nitroxide radicals $[8^{Cp}]^\bullet$, $[8^{\alpha}]^\bullet$, $[8^{\beta}]^\bullet$, $[8^1]^\bullet$, and $[8^2]^\bullet$ are quite similar in energy (Figure S7). The driving force for the formation of $[8^1]^\bullet$ from $[3-H^1]^\bullet$ and PhNO amounts to 81 kJ mol^{-1} (Figure S7). Hence, the product distribution is controlled by the relative stability of the *C*-centered radical $[3-H^1]^\bullet$ but not by the relative stability of the product nitroxide radical $[8^1]^\bullet$.

In order to gain insight into the reactivity of NH-containing ferrocenyl compounds, which are substructures of cytotoxic prodrugs **A** and **B** and antimalarial drugs **D** (Scheme 1),[7,9−13] we investigated the reactivity of the simple oxo- and thioamides, namely, *N*-acetylaminoferrocenium 4^+ (Scheme 3d), and *N*-thioacetylaminoferrocenium 5^+ in the presence of the $P_1{}^t$Bu base.

Because of the presence of five chemically different protons in **4**, five distinct radicals $[4-H^{Cp}]^\bullet$, $[4-H^{\alpha}]^\bullet$, $[4-H^{\beta}]^\bullet$, $[4-H^{N}]^\bullet$, and $[4-H^{Me}]^\bullet$ can be conceived in the radical pool $[4-H]^\bullet$ (Scheme 3d). The same holds analogously for **5**. This translates to the corresponding nitroxide radicals $[9^{Cp}]^\bullet$, $[9^{\alpha}]^\bullet$, $[9^{\beta}]^\bullet$, $[9^{N}]^\bullet$, and $[9^{Me}]^\bullet$ derived from 4^+ and PhNO and $[10^{Cp}]^\bullet$, $[10^{\alpha}]^\bullet$, $[10^{\beta}]^\bullet$, $[10^{N}]^\bullet$, and $[10^{Me}]^\bullet$ derived from the thioanalogue 5^+ and PhNO. Similar to the situation observed for $[8^1]^\bullet$, the room temperature EPR spectrum of $[9]^\bullet$ is rather well resolved, suggesting that only one or two nitroxide radical species are present (Figure 5). The main features of the

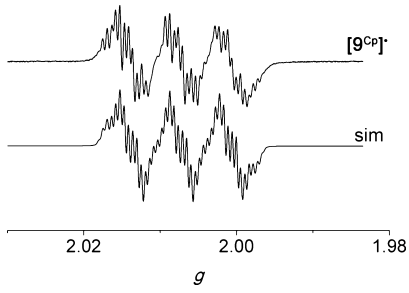

Figure 5. X-band EPR spectrum (top) and simulated spectrum (bottom) of $[9^{Cp}]^\bullet$ (25 mM **4** in CH_2Cl_2) at the following experimental parameters: temperature = 298 K, field = 3346.20 G, sweep = 94.79 G, sweep time = 90 s, modulation = 1000 mG, and MW attenuation = 10 dB.

experimental EPR resonance of $[9]^\bullet$ can be simulated by the expected hfc's to the PhNO moiety (^{14}N, H^o, H^m, H^p, Table 1) and coupling to four protons of 1.2 G (1H), 1.1 G (1H) and 0.70 G (2H). Further, small differences between the simulated and the experimental spectrum are associated with the presence of a second nitroxide radical with rather similar parameters. However, simulation of a full second parameter set would lead to severe overparametrization of the simulation. Hence, we note that the

DOI: 10.1021/acs.organomet.5b00778
Organometallics 2015, 34, 5310−5320

hfc's to ferrocene protons are less well-defined for $[\mathbf{9}]^{\bullet}$ than that for $[\mathbf{6}]^{\bullet}$, $[\mathbf{7}]^{\bullet}$, and $[\mathbf{8}^{\mathbf{1}}]^{\bullet}$. The presence of four protons close to the radical center suggest the $[\mathbf{9}^{\mathbf{Cp}}]^{\bullet}$ nitroxide radical derived from $[\mathbf{4}-\mathbf{H}^{\mathbf{Cp}}]^{\bullet}$ as the major trapped species (Figure 6). In $[\mathbf{9}^{\mathbf{Cp}}]^{\bullet}$, the hfc to H^{α} is smaller than that in $[\mathbf{6}]^{\bullet}$, and furthermore, two slightly different hfc's to chemically different H^{α} atoms are found for $[\mathbf{9}^{\mathbf{Cp}}]^{\bullet}$ (Table 1). The larger hfc to H^{α} in $[\mathbf{6}]^{\bullet}$ is easily traced back to the favorable coplanar orientation of the NO unit with the C_5H_4 ring (O−N−C^{ipso}-C^{α} = −23.0°) as compared to the corresponding torsion angle in $[\mathbf{9}^{\mathbf{Cp}}]^{\bullet}$ (O−N−C^{ipso}-C^{α} = −31.4°). The larger twist in $[\mathbf{9}^{\mathbf{Cp}}]^{\bullet}$ arises from an intramolecular NH(amide)···O(nitroxyl) hydrogen bond (Figure 6). Similar intramolecular hydrogen bonds have been amply observed in ferrocenyl polyamides.[48−51] This hydrogen bond furthermore provides a straightforward explanation for the chemically different $H^{\alpha}/H^{\alpha'}$ protons.

Expectedly, in the radical pool $[\mathbf{4}-\mathbf{H}]^{\bullet}$ the nitrogen-deprotonated radical $[\mathbf{4}-\mathbf{H}^{\mathbf{N}}]^{\bullet}$ is the most stable one (Figure S9). However, this radical is essentially iron-centered with a Mulliken spin density at iron of 1.248 with some small contribution of the nitrogen atom (Mulliken spin density at N 0.016). Attack of PhNO at iron is excluded based on the general lack of reactivity of ferrocenium ions toward PhNO. Attack of PhNO at the nitrogen atom of $[\mathbf{4}-\mathbf{H}^{\mathbf{N}}]^{\bullet}$ to give $[\mathbf{9}^{\mathbf{N}}]^{\bullet}$ is calculated to be disfavored by 37 kJ mol^{-1} relative to the starting materials $[\mathbf{4}-\mathbf{H}^{\mathbf{N}}]^{\bullet}$ and PhNO (Figure 6). A ring-slipped isomer $[\mathbf{4}-\mathbf{H}^{\mathbf{N}'}]^{\bullet}$ has been calculated as well, yet its spin density is also localized at the iron atom (Mulliken spin density at Fe 1.268), precluding the reaction of $[\mathbf{4}-\mathbf{H}^{\mathbf{N}'}]^{\bullet}$ with PhNO (Figure S9). The calculated ring-slipped structure of $[\mathbf{4}-\mathbf{H}^{\mathbf{N}'}]^{\bullet}$ suggests a viable decomposition pathway of radicals $[\mathbf{4}-\mathbf{H}]^{\bullet}$ releasing the substituted cyclopentadienyl ligand as *N*-acetyl-2,4-cyclopentadien-1-imine. Indeed, the formation of di(cyclopentadiene) and di(aminocyclopentadiene) has been observed in the reaction of prodrugs **A** with H_2O_2 (Scheme 1).[7]

In addition to these PhNO-resistant iron-centered radicals $[\mathbf{4}-\mathbf{H}^{\mathbf{N}}]^{\bullet}$ and $[\mathbf{4}-\mathbf{H}^{\mathbf{N}'}]^{\bullet}$, the radicals $[\mathbf{4}-\mathbf{H}^{\mathbf{Cp}}]^{\bullet}$, $[\mathbf{4}-\mathbf{H}^{\alpha}]^{\bullet}$, $[\mathbf{4}-\mathbf{H}^{\beta}]^{\bullet}$, and $[\mathbf{4}-\mathbf{H}^{\mathbf{Me}}]^{\bullet}$ deprotonated at carbon atoms were calculated by DFT (Figure S9). The reactions of $[\mathbf{4}-\mathbf{H}^{\mathbf{Cp}}]^{\bullet}$, $[\mathbf{4}-\mathbf{H}^{\alpha}]^{\bullet}$, $[\mathbf{4}-\mathbf{H}^{\beta}]^{\bullet}$, and $[\mathbf{4}-\mathbf{H}^{\mathbf{Me}}]^{\bullet}$ and PhNO to $[\mathbf{9}^{\mathbf{Cp}}]^{\bullet}$, $[\mathbf{9}^{\alpha}]^{\bullet}$, $[\mathbf{9}^{\beta}]^{\bullet}$, and $[\mathbf{9}^{\mathbf{Me}}]^{\bullet}$, respectively, are thermodynamically feasible (Figure 6). Interestingly, $[\mathbf{4}-\mathbf{H}^{\alpha}]^{\bullet}$ mainly features spin density at the iron center (Mulliken spin density at Fe 1.251) and is hence considered unreactive toward PhNO, so $[\mathbf{9}^{\alpha}]^{\bullet}$ should not be observed. In $[\mathbf{4}-\mathbf{H}^{\mathbf{Me}}]^{\bullet}$, the spin density is smeared over the nitrogen, oxygen, and CH_2 units of the substituent. This spin delocalization reduces the probability of PhNO attack, and hence, $[\mathbf{9}^{\mathbf{Me}}]^{\bullet}$ is not particularly favored as well. The remaining two highly reactive radicals $[\mathbf{4}-\mathbf{H}^{\mathbf{Cp}}]^{\bullet}$ and $[\mathbf{4}-\mathbf{H}^{\beta}]^{\bullet}$, although high in energy, might account for the observed EPR pattern with $[\mathbf{9}^{\mathbf{Cp}}]^{\bullet}$ derived from $[\mathbf{4}-\mathbf{H}^{\mathbf{Cp}}]^{\bullet}$ being the major and $[\mathbf{9}^{\beta}]^{\bullet}$ derived from $[\mathbf{4}-\mathbf{H}^{\beta}]^{\bullet}$ being the minor species based on simple statistical arguments. This interpretation agrees with the EPR spectral data. While the radicals $[\mathbf{4}-\mathbf{H}^{\mathbf{Cp}}]^{\bullet}$ and $[\mathbf{4}-\mathbf{H}^{\beta}]^{\bullet}$ of the radical pool can be trapped by PhNO, $[\mathbf{4}-\mathbf{H}^{\mathbf{N}}]^{\bullet}$ and $[\mathbf{4}-\mathbf{H}^{\mathbf{N}'}]^{\bullet}$ are inert toward PhNO. In order to possibly detect the rather persistent and PhNO-resistant Fe-centered radical $[\mathbf{4}-\mathbf{H}^{\mathbf{N}}]^{\bullet}$, rapid-freeze EPR techniques have been employed.

The EPR spectrum recorded at 77 K rapidly after deprotonation of $\mathbf{4}^{+}$ in the presence of PhNO shows a characteristic broad ferrocenium-based resonance (83%) in addition to the slightly anisotropic nitrogen-split triplet resonance of a nitroxide radical with one large hfc to ^{14}N (17%) (Figure 7 and Table 2). The latter EPR resonance is very similar to the corresponding resonance of $[\mathbf{6}]^{\bullet}$ and is hence safely

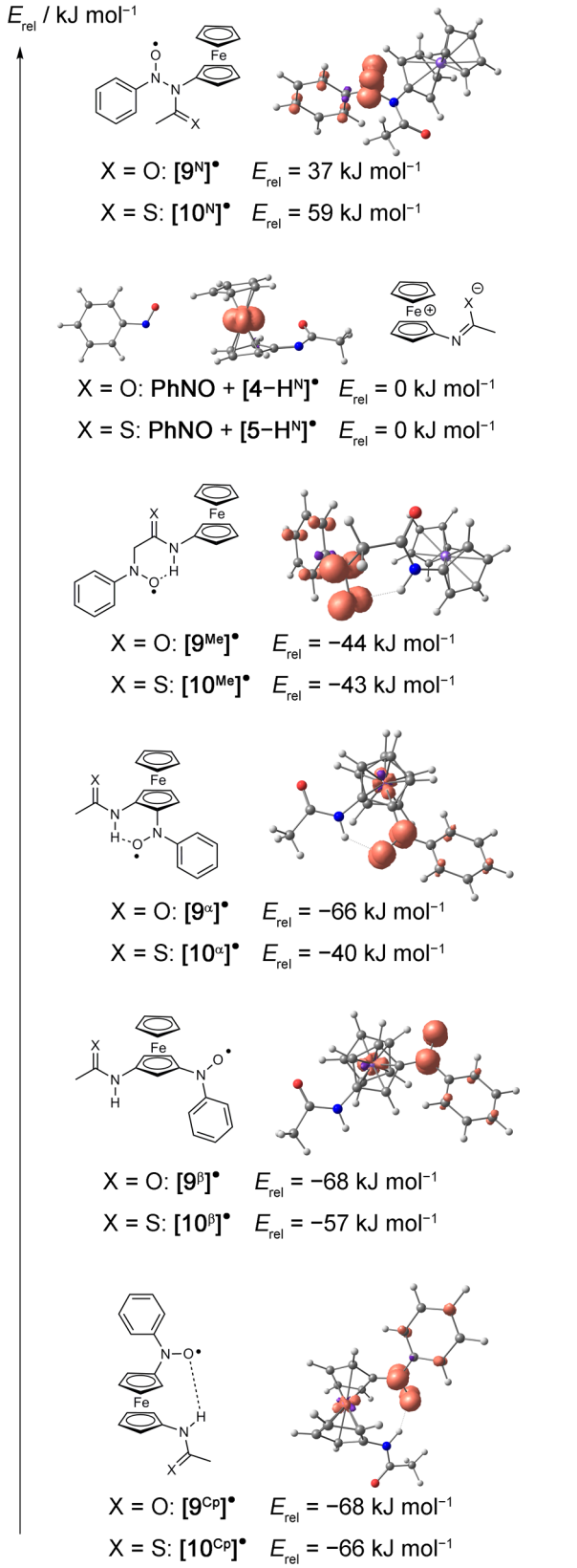

Figure 6. DFT optimized geometries with spin densities for $[\mathbf{9}^{\mathbf{x}}]^{\bullet}$ (x = α, β, Cp, N, and Me) (0.01 au isosurface value) and energies in CH_2Cl_2 continuum solvent for $[\mathbf{9}^{\mathbf{x}}]^{\bullet}$ and $[\mathbf{10}^{\mathbf{x}}]^{\bullet}$ (x = α, β, Cp, N, and Me) as well as Lewis structures.

DOI: 10.1021/acs.organomet.5b00778
Organometallics 2015, 34, 5310−5320

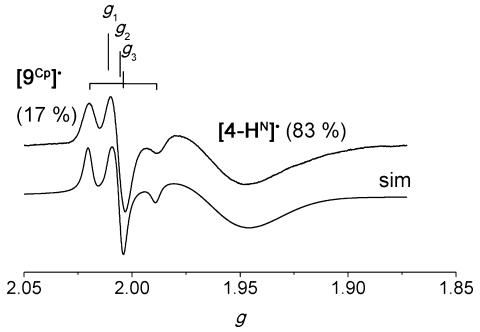

Figure 7. X-band EPR spectrum (top) and simulated spectrum (bottom) of $[\mathbf{9}^{Cp}]^{\bullet}/[\mathbf{4}{-}\mathbf{H}^{N}]^{\bullet}$ (25 mM **4** in CH_2Cl_2) at the following experimental parameters: temperature = 77 K, field = 3346.20 G, sweep = 499.77 G, sweep time = 90 s, modulation = 5000 mG, and MW attenuation = 10 dB.

assigned to already formed nitroxide radicals $[\mathbf{9}^{Cp/\beta}]^{\bullet}$. The broad ferrocenium resonance ($g_{1,2,3}$ = N/A, 1.9650, and 1.9400, Table 2), however, clearly differs from the EPR resonance of the ferrocenium ion $\mathbf{4}^{+}$ ($g_{1,2,3}$ = 3.3500, 1.8750, and 1.7870).[35] Hence, the resonance is assigned to $[\mathbf{4}{-}\mathbf{H}^{N}]^{\bullet}$. This iron-centered radical is unable to react with PhNO itself but equilibrates with radical species deprotonated at carbon atoms $[\mathbf{4}{-}\mathbf{H}^{x}]^{\bullet}$ (x = α, β, Cp, Me). After annealing the sample to room temperature for 5 min and refreezing to 77 K, the ferrocenium resonance of $[\mathbf{4}{-}\mathbf{H}^{N}]^{\bullet}$ has vanished, and only the resonance of the nitroxide radicals $[\mathbf{9}^{Cp/\beta}]^{\bullet}$ remained.

In the absence of PhNO, rapid-freeze EPR spectroscopy of the $\mathbf{4}^{+}/P_1{}^{t}Bu$ mixture yields an EPR spectrum displaying the resonance assigned to $[\mathbf{4}{-}\mathbf{H}^{N}]^{\bullet}$ (99.2%) (Figure S8a). This finding supports the above assignment. Furthermore, a weak but significant slightly anisotropic resonance at g = 2.0 without resolved hyperfine couplings is detected (0.8%) (Table 2, Figure S8a). This resonance is assigned to traces of the carbon-centered radicals $[\mathbf{4}{-}\mathbf{H}^{x}]^{\bullet}$ (x = α, β, Cp, Me) of the radical pool $[\mathbf{4}{-}\mathbf{H}]^{\bullet}$ (Table 2). At room temperature, this sample exhibits a transient EPR resonance without discernible hfc's at g_{iso} = 2.0078 (Figure S8b) which is assigned to the *C*-centered radicals $[\mathbf{4}{-}\mathbf{H}^{x}]^{\bullet}$ (x = α, β, Cp, Me) as well. The proposed reactivity of $\mathbf{4}^{+}$ in the presence of a base is summarized in Scheme 5. Deprotonation of $\mathbf{4}^{+}$ gives the radical pool $[\mathbf{4}{-}\mathbf{H}]^{\bullet}$ with $[\mathbf{4}{-}\mathbf{H}^{N}]^{\bullet}$ being the most stable and abundant radical (99.2%). Neither $\mathbf{4}^{+}$ nor $[\mathbf{4}{-}\mathbf{H}^{N}]^{\bullet}$ react with PhNO. Less than one percent of the observed radicals are carbon-centered radicals $[\mathbf{4}{-}\mathbf{H}^{x}]^{\bullet}$ (x = α, β, Cp, Me). However, two of these, namely, $[\mathbf{4}{-}\mathbf{H}^{Cp}]^{\bullet}$ and $[\mathbf{4}{-}\mathbf{H}^{\beta}]^{\bullet}$, can be trapped by PhNO to give the respective nitroxide radicals $[\mathbf{9}^{Cp}]^{\bullet}$ and $[\mathbf{9}^{\beta}]^{\bullet}$. Quantification[52] of the nitroxide radical species $[\mathbf{9}^{Cp}]^{\bullet}$ and $[\mathbf{9}^{\beta}]^{\bullet}$ with respect to external calibration with DPPH reveals that indeed less than 1% of the original ferrocenium radical $\mathbf{4}^{+}$ is transformed into the nitroxides $[\mathbf{9}^{Cp}]^{\bullet}$ and $[\mathbf{9}^{\beta}]^{\bullet}$. One possible decomposition pathway of the radicals via the ring-slipped isomer $[\mathbf{4}{-}\mathbf{H}^{N'}]^{\bullet}$ is proposed on the basis of DFT calculations of $[\mathbf{4}{-}\mathbf{H}^{N'}]^{\bullet}$. Further radical reactivity might be hydrogen atom abstraction from the solvent or the base to give the starting material **4**. Indeed, quenching the radical pool $[\mathbf{4}{-}\mathbf{H}]^{\bullet}$ by hydrazine hydrate essentially quantitatively recovers ferrocene **4** as shown by ^{1}H NMR spectroscopy.

The successful deprotonation of $\mathbf{4}^{+}$ to the radical pool $[\mathbf{4}{-}\mathbf{H}]^{\bullet}$ is furthermore evidenced by cyclic voltammetry. At 298 K in $CH_2Cl_2/[^{n}Bu_4N][B(C_6F_5)_4]$, a reversible one-electron process is observed at $E_{1/2}$ = −50 mV vs FcH/FcH$^+$ and assigned to the **4**/$\mathbf{4}^{+}$ couple (Figure S10a). After the addition of stoichiometric amounts of $P_1{}^{t}Bu$, this process is replaced by an irreversible oxidation at E_p = −175 mV vs FcH/FcH$^+$ (Figure S10b). The lower potential of the **4**/$\mathbf{4}^{+}$ couple in the presence of $P_1{}^{t}Bu$ is ascribed to coordination of the base to the amide unit of **4** via a hydrogen bond. Oxidation to $\mathbf{4}^{+}$ acidifies this NH proton, and the proton is transferred to the base giving the radicals $[\mathbf{4}{-}\mathbf{H}]^{\bullet}$, with $[\mathbf{4}{-}\mathbf{H}^{N}]^{\bullet}$ being the major product. Reduction of the rather persistent radical $[\mathbf{4}{-}\mathbf{H}^{N}]^{\bullet}$ occurs at E_p' = −890 mV vs FcH/FcH$^+$ (Figure S10b). These results reflect the intimate coupling of proton transfer and electron transfer reactions in ferrocenium amides as reported in the literature.[35,49−51]

Scheme 5. Suggested Radical Reactivity of $\mathbf{4}^{+}$ in the Presence of a Base and PhNO[a]

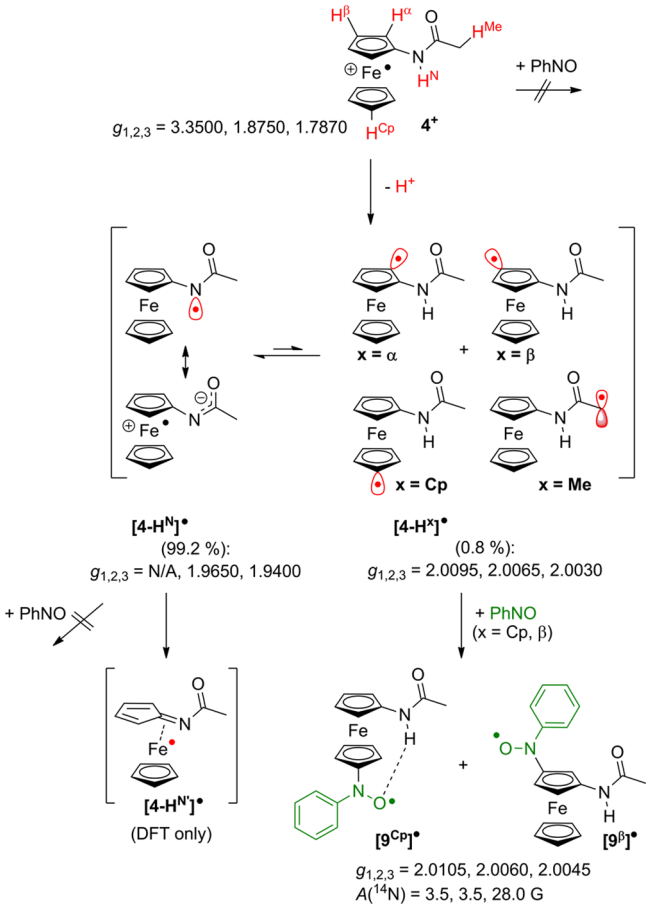

[a]EPR data (77 K) of identified intermediates are given.

In order to investigate the effect of O → S exchange in the amide for the spin trapping experiments in the presence of $P_1{}^{t}Bu$, we employed thioamide **5** as the sulfur analogue of **4**.[51] Similar to $\mathbf{4}^{+}$, a radical pool $[\mathbf{5}{-}\mathbf{H}^{Cp}]^{\bullet}$, $[\mathbf{5}{-}\mathbf{H}^{\alpha}]^{\bullet}$, $[\mathbf{5}{-}\mathbf{H}^{\beta}]^{\bullet}$, $[\mathbf{5}{-}\mathbf{H}^{N}]^{\bullet}$, and $[\mathbf{5}{-}\mathbf{H}^{Me}]^{\bullet}$ is established after deprotonation of $\mathbf{5}^{+}$ (Scheme 5) Fully paralleling the energies of the corresponding radicals $[\mathbf{4}{-}\mathbf{H}]^{\bullet}$, the most stable one is the iron-centered radical $[\mathbf{5}{-}\mathbf{H}^{N}]^{\bullet}$ (Figure S9), while the ring and side chain radicals $[\mathbf{5}{-}\mathbf{H}^{Cp}]^{\bullet}$, $[\mathbf{5}{-}\mathbf{H}^{\alpha}]^{\bullet}$, $[\mathbf{5}{-}\mathbf{H}^{\beta}]^{\bullet}$, and $[\mathbf{5}{-}\mathbf{H}^{Me}]^{\bullet}$ are higher in energy.

The EPR spectrum obtained from the $\mathbf{5}^{+}$/PhNO/$P_1{}^{t}Bu$ mixture at room temperature is very well simulated by a single set of parameters (Figure 8 and Table 1). The hfc's are consistent with the nitroxide radical $[\mathbf{10}^{Cp}]^{\bullet}$. Similar to $[\mathbf{9}^{Cp}]^{\bullet}$, hyperfine coupling to the H^{α} atoms is split due to the chemical dissimilarity of H^{α} and $H^{\alpha'}$ in $[\mathbf{10}^{Cp}]^{\bullet}$ featuring an intramolecular

DOI: 10.1021/acs.organomet.5b00778
Organometallics 2015, 34, 5310−5320

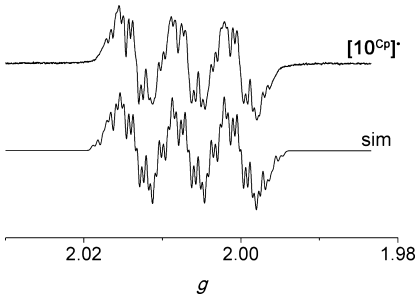

Figure 8. X-band EPR spectrum (top) and simulated spectrum (bottom) of $[\mathbf{10}^{Cp}]^{\bullet}$ (25 mM **5** in CH_2Cl_2) at the following experimental parameters: temperature = 298 K, field = 3346.20 G, sweep = 94.79 G, sweep time = 90 s, modulation = 1000 mG, and MW attenuation = 10 dB.

NH(thioamide)···O(nitroxide) hydrogen bond (Figure 6). According to the DFT calculations, this hydrogen bond is shorter in $[\mathbf{10}^{Cp}]^{\bullet}$ (NH···O 1.885 Å) than that in $[\mathbf{9}^{Cp}]^{\bullet}$ (NH···O 1.984 Å), suggesting a stronger bond in $[\mathbf{10}^{Cp}]^{\bullet}$ in agreement with the increased acidity of thioamides.[51] The stronger intramolecular hydrogen bond might also lead to a more pronounced differentiation between H^{α} and $H^{\alpha'}$. In fact, even the β-hydrogen atoms become chemically inequivalent and yield different hfc's in $[\mathbf{10}^{Cp}]^{\bullet}$ (Table 1). The larger hfc to $H^{\alpha}/H^{\alpha'}$ in $[\mathbf{10}^{Cp}]^{\bullet}$ than in $[\mathbf{9}^{Cp}]^{\bullet}$ might be associated with the smaller torsion angle $O-N-C^{ipso}-C^{\alpha} = -25.1°$ in $[\mathbf{10}^{Cp}]^{\bullet}$.

In order to observe iron-centered radicals, the $\mathbf{5}^{+}$/PhNO/$P_1{}^t$Bu reaction mixture was subjected to EPR spectroscopy at 77 K (Figure 9). The EPR spectrum displays three discernible

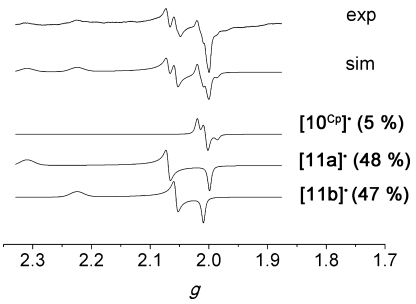

Figure 9. X-band EPR spectrum (exp) and simulated spectrum (sim) of $[\mathbf{10}^{Cp}]^{\bullet}$ consisting of three components $[\mathbf{10}^{Cp}]^{\bullet}$, $[\mathbf{11a}]^{\bullet}$, and $[\mathbf{11b}]^{\bullet}$; (5 mM **5** in CH_2Cl_2) at the following experimental parameters: temperature = 77 K, field = 3245.45 G, sweep = 697.96 G, sweep time = 90 s, modulation = 5000 mG, MW attenuation = 10 dB.

resonances. One resonance originates from the spin trapped product $[\mathbf{10}^{Cp}]^{\bullet}$ (5%) bearing close resemblance to the resonance of the amide nitroxide radical $[\mathbf{9}^{Cp}]^{\bullet}$ (Table 2). The other two rhombic resonances, present in nearly equal intensities (48%; 47%; Table 2), appear to correlate to follow-up products $[\mathbf{11a}]^{\bullet}$ and $[\mathbf{11b}]^{\bullet}$ of the initially formed radicals $[\mathbf{5-H}]^{\bullet}$. The identity of these follow-up products is as yet unknown. In the absence of PhNO, the resonances of these follow-up products $[\mathbf{11a}]^{\bullet}$ and $[\mathbf{11b}]^{\bullet}$ are observed as well (Figure 10). This finding eliminates a reaction with PhNO as being responsible for the formation of $[\mathbf{11a}]^{\bullet}$ and $[\mathbf{11b}]^{\bullet}$. In the absence of PhNO, the resonance of the $\mathbf{5}^{+}$ cation[51] is observed additionally (Table 2 and Figure 10). Hence, $[\mathbf{11a}]^{\bullet}$ and $[\mathbf{11b}]^{\bullet}$ seem to be associated with follow-up products of the sulfur substituent $[\mathbf{5-H}]^{\bullet}$, independent of the presence of PhNO.

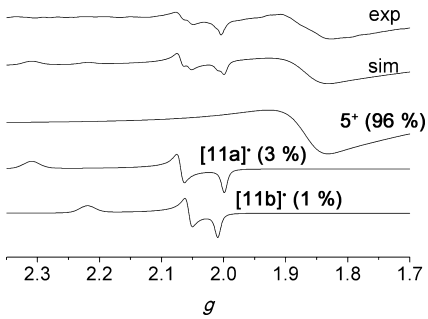

Figure 10. X-band EPR spectrum (exp) and simulated spectrum (sim) of $\mathbf{5}^{+}/P_1{}^t$Bu consisting of three components, $\mathbf{5}^{+}$, $[\mathbf{11a}]^{\bullet}$, and $[\mathbf{11b}]^{\bullet}$ (5 mM **5** in CH_2Cl_2) at the following experimental parameters: temperature = 77 K, field = 2499.01 G, sweep = 3989.53 G, sweep time = 120 s, modulation = 3000 mG, and MW attenuation = 10 dB.

While it has been reported previously that the chemical reactivity and properties of ferrocenyl thioamides can differ from the chemistry of the corresponding amides,[51] *C*-radical reactivity in the presented spin trapping reaction results in the analogous product(s) $[\mathbf{9}^{Cp/\beta}]^{\bullet}$ and $[\mathbf{10}^{Cp}]^{\bullet}$. Yet, the sulfur atom appears to open further reaction pathways yielding radicals $[\mathbf{11a}]^{\bullet}$ and $[\mathbf{11b}]^{\bullet}$. Their investigation is beyond the scope of the present study and will be reported elsewhere.

Obviously, oxidized ferrocenyl amides and thioamides $\mathbf{4}^{+}$ and $\mathbf{5}^{+}$ can be easily deprotonated at their respective nitrogen atoms yielding the metal centered radicals $[\mathbf{4-H}^{N}]^{\bullet}$ (observed by rapid-freeze EPR) and $[\mathbf{5-H}^{N}]^{\bullet}$. These iron-centered radicals are even resistant toward reaction with PhNO. Yet, the *N*-deprotonated tautomers $[\mathbf{4-H}^{N}]^{\bullet}$ and $[\mathbf{5-H}^{N}]^{\bullet}$ can isomerize to reactive *C*-deprotonated species $[\mathbf{4-H}^{x}]^{\bullet}$ and $[\mathbf{5-H}^{x}]^{\bullet}$ to a small extent (x = α, β, Cp, Me). Some of these *C*-centered radicals, $[\mathbf{4-H}^{x}]^{\bullet}$ and $[\mathbf{5-H}^{x}]^{\bullet}$, can be trapped by PhNO (<1%) to give the stable nitroxyl radicals $[\mathbf{9}^{Cp/\beta}]^{\bullet}$ and $[\mathbf{10}^{Cp}]^{\bullet}$. In the presence of a base, even two more radical species, $[\mathbf{11a}]^{\bullet}$ and $[\mathbf{11b}]^{\bullet}$, are detected for the sulfur derivative $\mathbf{5}^{+}$ by EPR in the reaction mixture. Radicals $[\mathbf{11a}]^{\bullet}$ and $[\mathbf{11b}]^{\bullet}$ are inert toward PhNO, similar to other ferrocenium radicals $\mathbf{1}^{+}-\mathbf{5}^{+}$. It appears that Fc-NHC(X)R can be oxidized to the rather stable conjugate acid/base pair $[Fc\text{-}NHC(X)R]^{+}/[Fc\text{-}NC(X)R]^{\bullet}$ (X = O, S). *C*-Centered reactive radicals are then slowly formed via intramolecular proton-coupled electron transfer (PCET) or hydrogen atom transfer (Scheme 5).[53−64]

In the PCET reaction, a proton is transferred from a cyclopentadienyl carbon atom to the nitrogen atom, while an electron from the original CH bond is transferred to the iron(III) center. Hence, $\mathbf{4}^{+}/[\mathbf{4-H}^{N}]^{\bullet}$ and $\mathbf{5}^{+}/[\mathbf{5-H}^{N}]^{\bullet}$ might act as a reservoir for reactive *C*-centered radicals (maybe even under physiological conditions). This might also explain some of the enhanced biological reactivity patterns observed for amino ferrocene based drugs and prodrugs such as **A**, **B**, or **D** (Scheme 1). *C*-Centered radicals have also been proposed for the active species derived from ferrocifen **F** (Scheme 1). Hence, a common feature of such biologically active ferrocene/ferrocenium species might be the presence of some ionizable NH/OH group close to the ferrocenium site, suggesting an intimate coupling of electron and proton transfer to generate metastable iron-centered radicals. Highly reactive carbon-centered radicals might then be formed from these species in small amounts via intramolecular proton-coupled electron transfer reactions. These might account for further biological effects.

DOI: 10.1021/acs.organomet.5b00778
Organometallics 2015, 34, 5310−5320

CONCLUSIONS

In contrast to other 17 valence electron metal centered radicals, such as $[Mn(CO)_5]^\bullet$, ferrocenium ions are inert toward the reaction with the spin trapping agent nitrosobenzene. However, in the presence of a suitable base, small amounts of carbon-centered radicals are generated. Some of these reactive radicals add to nitrosobenzene giving the respective stable nitroxide radicals. EPR spectra of the corresponding stable ferrocenyl phenyl nitroxide radicals clearly reveal the position of the original radical site, namely, C_5H_5 for ferrocene, CH_3 for decamethylferrocene, and CH_2 for ethylferrocene. The most acidic site in $NHC(X)CH_3$ substituted ferrocene/ferrocenium couples (X = O, S) is the NH group, and iron-centered radicals are formed according to EPR studies. Again, these iron-centered radicals do not add to nitrosobenzene. Yet, small amounts of *C*-deprotonated tautomers generated from the *N*-deprotonated, iron-centered radicals are trapped by attack of nitrosobenzene at the Cp rings. Hence, these stable and inert $NHC(X)CH_3$ substituted ferrocene/ferrocenium couples slowly release reactive *C*-centered radicals and can thus be considered as a reservoir for reactive radicals. This reactivity might also be of importance in the biological mode of action of OH/NH-substituted ferrocene-based drugs and prodrugs, such as ferrocifen, ferroquine, and related compounds.

EXPERIMENTAL SECTION

General Considerations. All reactions were performed under argon atmosphere unless otherwise noted. Dichloromethane was dried over CaH_2 and distilled prior to use. Ferrocene (**1**) was commercially available from Acros. Decamethylferrocene (**2**) was used as received from ABCR. Ethylferrocene (**3**), P_1^tBu, 2,2-diphenyl-1-picrylhydrazyl (DPPH), and nitrosobenzene (PhNO) were commercially available from Sigma-Aldrich. *N*-Acetylaminoferrocene (**4**),[65] *N*-thioacetylaminoferrocene (**5**),[51] and $[^nBu_4N][B(C_6F_5)_4]$[42,43] were prepared according to literature procedures. Filtrations from precipitated silver after oxidation were performed with syringe filters (Rotilabo-Spritzenfilter, Ø = 15 mm, pore size = 0.20 μm; Carl Roth GmbH + Co. KG, Germany). Electrochemical experiments were carried out on a BioLogic SP-50 voltammetric analyzer using a platinum working electrode, a platinum wire as counter electrode, and a 0.01 M $Ag/AgNO_3$ electrode as reference electrode. The measurements were carried out at a scan rate of 100 mV s^{-1} for cyclic voltammetry experiments and for square wave voltammetry experiments unless noted otherwise using 0.1 M $[^nBu_4N][B(C_6F_5)_4]$ as supporting electrolyte and 0.001 M solution of the sample in CH_2Cl_2. Potentials are given relative to the ferrocene/ferrocenium couple. Referencing was achieved by addition of ferrocene or decamethylcobaltocene ($E_{1/2}$ = −2.04 V vs FcH/FcH^+ (CH_2Cl_2; $[^nBu_4N][B(C_6F_5)_4]$)) to the sample.[42,43] CW EPR spectra (X-band; ca. 9.4 GHz) were measured on a Miniscope MS 300 at 298 K and at 77 K cooled by liquid nitrogen in a finger dewar (Magnettech GmbH, Berlin, Germany). Settings are given at the respective displayed spectra. *g*-Values are referenced to external Mn^{2+} in ZnS (*g* = 2.118, 2.066, 2.027, 1.986, 1.946, and 1.906). Simulations of EPR spectra were performed with EasySpin (v 5.0.0)[66] for MatLab (R2015a). For quantification measurements, EPR tubes with an internal diameter of 2.0 mm were used. The calibration curve was determined using commercially available 2,2-diphenyl-1-picrylhydrazyl (DPPH) as standard. The samples were prepared in a glovebox under argon, and the EPR tubes were filled with 400 μL of the solution and sealed with Critoseal. They were inserted 10.4 cm (measured at the Teflon holder) into the EPR spectrometer. Three concentrations (0.03, 0.01, and 0.005 mM) in CH_2Cl_2 were used for the calibration. The settings for the calibration curve and the sample EPR spectra were as follows: temperature = 298 K, field = 3346.20 G, sweep = 94.79 G, sweep time = 90 s, modulation = 5000 mG, MW attenuation = 10 db, and number of passes = 3. For an estimation of the error at the insertion of the EPR tube into the spectrometer cavity, the sample with 0.03 mM concentration was inserted, measured, reinserted, and measured three times. For the *c* = 0.03 mM sample, a variation of 13% between highest and lowest value of the three measurements after double integration is obtained. Baseline correction was achieved with EasySpin[66] for MatLab with normalization turned off. The obtained spectra were integrated twice with Origin Pro 8.0, and the double integral values were plotted against the concentration (Figures S11 and S12).

Density Functional Calculations. These were carried out with the ORCA 3.0.2/DFT series[67] of programs. For geometry optimizations and energy calculations, the B3LYP formulation of density functional theory was used employing the SV(P)[68,69] basis set, the RIJCOSX approximation, approximate Second Order SCF (SOSCF),[70,71] the zeroth order regular approximation (ZORA),[72−74] and the KDIIS algorithm, at GRIDX4. No symmetry constraints were imposed on the molecules. The presence of energy minima of the ground states was checked by numerical frequency calculations. Solvent modeling was done employing the conductor like screening model (COSMO, CH_2Cl_2).[75] The approximate free energies at 298 K were obtained through thermochemical analysis of the frequency calculation, using the thermal correction to Gibbs free energy as reported by ORCA 3.0.2.

ASSOCIATED CONTENT

Supporting Information

The Supporting Information is available free of charge on the ACS Publications website at DOI: 10.1021/acs.organomet.5b00778.

Square wave and cyclic voltammograms of P_1^tBu, **1**, **1**/P_1^tBu, **4**, and **4**/P_1^tBu in $CH_2Cl_2/[^nBu_4N][B(C_6F_5)_4]$ at 298 K, DFT optimized geometry and spin density in CH_2Cl_2 for $[\mathbf{1\text{-}PhNO}]^+$, $[\mathbf{1{-}H}]^\bullet$, $[\mathbf{2{-}H}]^\bullet$, $[\mathbf{3{-}H^x}]^\bullet$ (x = α, β, Cp, 1, 2), $[\mathbf{8^x}]^\bullet$ (x = α, β, Cp, 1, 2), $[\mathbf{4{-}H^x}]^\bullet$ and $[\mathbf{5{-}H^x}]^\bullet$ (x = α, β, Cp, N, Me), and $[\mathbf{4{-}H^{N\prime}}]^\bullet$; EPR spectra and simulations in CH_2Cl_2 at 77 K of $[\mathbf{6}]^\bullet$, $[\mathbf{7}]^\bullet$, $[\mathbf{8^1}]^\bullet$, $[\mathbf{4{-}H^N}]^\bullet$, and $[\mathbf{4{-}H^x}]^\bullet$ (x = α, β, Cp, Me), and at 298 K of $[\mathbf{4{-}H^x}]^\bullet$ (x = α, β, Cp, Me); EPR spectra of quantification experiments in CH_2Cl_2 at 298 K of $[\mathbf{6}]^\bullet$, $[\mathbf{7}]^\bullet$, $[\mathbf{8^1}]^\bullet$, $[\mathbf{9^{Cp/\beta}}]^\bullet$, $[\mathbf{10^{Cp}}]^\bullet$, and DPPH in 0.03 mM, 0.01 mM, and 0.005 mM concentration, and Cartesian coordinates of optimized structures (PDF)

Cartesian Coordinates of all DFT optimzed structures in .xyz format (XYZ)

AUTHOR INFORMATION

Corresponding Author

*E-mail: katja.heinze@uni-mainz.de.

Author Contributions

†A.N. and T.K. contributed equally to the manuscript.

Notes

The authors declare no competing financial interest.

ACKNOWLEDGMENTS

We are grateful to Dipl.-Chem. Christoph Kreitner for his helpful remarks concerning DFT calculations. Parts of this research were conducted using the supercomputer Mogon and advisory services offered by Johannes Gutenberg University Mainz (www.hpc.uni-mainz.de), which is a member of the AHRP and the Gauss Alliance e.V.

REFERENCES

(1) Special issue on ferrocene chemistry: Heinze, K.; Lang, H. *Organometallics* **2013**, *32*, 5623−5625.

(2) Special issue on ferrocene chemistry: Adams, R. D. *J. Organomet. Chem.* **2001**, *637*−*639*, 1.

DOI: 10.1021/acs.organomet.5b00778
Organometallics 2015, 34, 5310−5320

(3) (a) Togni, A.; Hayashi, T. *Ferrocenes*; Togni, A., Hayashi, T., Eds.; VCH: Weinheim, Germany, 1995. (b) Stepnicka, P., Ed., *Ferrocenes: Ligands, Materials and Biomolecules*; VCH: Weinheim, Germany, 2008.
(4) Ornelas, C. *New J. Chem.* **2011**, *35*, 1973−1985.
(5) Gasser, G.; Ott, I.; Metzler-Nolte, N. *J. Med. Chem.* **2011**, *54*, 3−25.
(6) Tabbì, G.; Cassino, C.; Cavigiolio, G.; Colangelo, D.; Ghiglia, A.; Viano, I.; Osella, D. *J. Med. Chem.* **2002**, *45*, 5786−5796.
(7) Hagen, H.; Marzenell, P.; Jentzsch, E.; Wenz, F.; Veldwijk, M. R.; Mokhir, A. *J. Med. Chem.* **2012**, *55*, 924−934.
(8) Osella, D.; Ferrali, M.; Zanello, P.; Laschi, F.; Fontani, M.; Nervi, C.; Cavigiolio, G. *Inorg. Chim. Acta* **2000**, *306*, 42−48.
(9) Marzenell, P.; Hagen, H.; Sellner, L.; Zenz, T.; Grinyte, R.; Pavlov, V.; Daum, S.; Mokhir, A. *J. Med. Chem.* **2013**, *56*, 6935−6944.
(10) Daum, S.; Chekhun, V. F.; Todor, I. N.; Lukianova, N. Y.; Shvets, Y. V.; Sellner, L.; Putzker, K.; Lewis, J.; Zenz, T.; de Graaf, I. A. M.; Groothuis, G. M. M.; Casini, A.; Zozulia, O.; Hampel, F.; Mokhir, A. *J. Med. Chem.* **2015**, *58*, 2015−2024.
(11) Dubar, F.; Slomianny, C.; Khalife, J.; Dive, D.; Kalamou, H.; Guérardel, Y.; Grellier, P.; Biot, C. *Angew. Chem.* **2013**, *125*, 7844−7847; *Angew. Chem., Int. Ed.* **2013**, *52*, 7690−7693.
(12) Biot, C.; Nosten, F.; Fraisse, L.; Ter-Minassian, D.; Khalife, J.; Dive, D. *Parasite* **2011**, *18*, 207−214.
(13) Biot, C.; Glorian, G.; Maciejewski, L. A.; Brocard, J. S.; Domaire, O.; Blampain, G.; Millet, P.; Georges, A. J.; Abessolo, H.; Dive, D.; Lebibi, J. *J. Med. Chem.* **1997**, *40*, 3715−3718.
(14) Zanellato, I.; Heldt, J.-M.; Vessières, A.; Jaouen, G.; Osella, D. *Inorg. Chim. Acta* **2009**, *362*, 4037−4042.
(15) Hamels, D.; Dansette, P. M.; Hillard, E. A.; Top, S.; Vessières, A.; Herson, P.; Jaouen, G.; Mansuy, D. *Angew. Chem.* **2009**, *121*, 9288−9290; *Angew. Chem., Int. Ed.* **2009**, *48*, 9124−9126.
(16) Hillard, E.; Vessières, A.; Thouin, L.; Jaouen, G.; Amatore, C. *Angew. Chem.* **2006**, *118*, 291−296; *Angew. Chem., Int. Ed.* **2006**, *45*, 285−290.
(17) Jaouen, G.; Top, S.; Vessieres, A.; Leclercq, G.; McGlinchey, M. *Curr. Med. Chem.* **2004**, *11*, 2505−2517.
(18) Nguyen, A.; Top, S.; Pigeon, P.; Vessières, A.; Hillard, E. a.; Plamont, M. A.; Huché, M.; Rigamonti, C.; Jaouen, G. *Chem. - Eur. J.* **2009**, *15*, 684−696.
(19) Michard, Q.; Jaouen, G.; Vessieres, A.; Bernard, B. A. *J. Inorg. Biochem.* **2008**, *102*, 1980−1985.
(20) Osella, D.; Mahboobi, H.; Colangelo, D.; Cavigiolio, G.; Vessières, A.; Jaouen, G. *Inorg. Chim. Acta* **2005**, *358*, 1993−1998.
(21) Abramovitch, R. A.; Azogu, C. I.; Sutherland, R. G. *J. Chem. Soc. D* **1971**, 134−135.
(22) Jackson, R. A.; Scarmoutsos, M.; Zarkadis, A. K. *J. Chem. Soc., Perkin Trans. 2* **1991**, *2*, 809−810.
(23) (a) Cais, M.; Ashkenazi, P.; Dane, S.; Gottlieb, J. *J. Organomet. Chem.* **1976**, *122*, 403−411. (b) Creary, X. *Org. Lett.* **2000**, *2*, 2069−2072.
(24) Neuse, E. W. *J. Macromol. Sci., Chem.* **1981**, *16*, 3−72.
(25) Taniguchi, N.; Uemura, M. *Tetrahedron Lett.* **1998**, *39*, 5385−5388.
(26) Ashkenazi, P.; Cais, M. *Angew. Chem.* **1972**, *84*, 1106−1107; *Angew. Chem., Int. Ed. Engl.* **1972**, *11*, 1027−1028.
(27) Hudson, A.; Lappert, M. F.; Lednor, P. W.; Nicholson, B. K. *J. Chem. Soc., Chem. Commun.* **1974**, 966−967.
(28) Huffadine, A. S.; Dawson, P. A.; Peake, B. M.; Robinson, B. H.; Simpson, J. *J. Organomet. Chem.* **1976**, *121*, 391−403.
(29) Benner, L. S.; Balch, A. L. *J. Organomet. Chem.* **1977**, *134*, 121−130.
(30) Hudson, A.; Lappert, M. F.; Nicholson, B. K. *J. Chem. Soc., Dalton Trans.* **1977**, 551−554.
(31) (a) Forrester, A. R.; Hepburn, P.; Dunlop, R. S.; Mills, H. H. *J. Chem. Soc. D* **1969**, 698−699. (b) Elschenbroich, C.; Cais, M. *J. Organomet. Chem.* **1969**, *18*, 135−143. (c) Alberti, A.; Benaglia, M.; Bonini, B. F.; Fochi, M.; Macciantelli, D.; Marcaccio; Paolucci, F.; Roffia, S. *J. Phys. Org. Chem.* **2004**, *17*, 1084−1090.
(32) Babin, V. N.; Belousov, Y. A.; Belousova, T. A.; Borisov, Y. A.; Gumenyuk, V. V.; Nekrasov, Y. S. *Russ. Chem. Bull.* **2011**, *60*, 2081−2087.
(33) (a) Connelly, N. G.; Geiger, W. E. *Chem. Rev.* **1996**, *96*, 877−910. (b) Fujita, E.; Gordon, B.; Hillman, M.; Nagy, A. G. *J. Organomet. Chem.* **1981**, *218*, 105−114.
(34) Prins, R. *Mol. Phys.* **1970**, *19*, 603−620.
(35) Neidlinger, A.; Ksenofontov, V.; Heinze, K. *Organometallics* **2013**, *32*, 5955−5965.
(36) Kondo, Y. In *Supberbases for Organic Synthesis*; Ishikawa, T., Ed.; John Wiley & Sons, Ltd: Chichester, UK, 2009; pp 145−185.
(37) Barclay, L. R. C.; Dust, J. M. *Can. J. Chem.* **1982**, *60*, 607−615.
(38) Omelka, L.; Kováčová, J. *Magn. Reson. Chem.* **1994**, *32*, 525−531.
(39) Cais, M.; Ashkenazi, P.; Dani, S.; Gottlieb, J. *J. Organomet. Chem.* **1977**, *124*, 49−58.
(40) Buettner, G. R. *Free Radical Biol. Med.* **1987**, *3*, 259−303.
(41) Huesmann, H.; Förster, C.; Siebler, D.; Gasi, T.; Heinze, K. *Organometallics* **2012**, *31*, 413−427.
(42) LeSuer, R. J.; Buttolph, C.; Geiger, W. E. *Anal. Chem.* **2004**, *76*, 6395−6401.
(43) Camire, N.; Mueller-Westerhoff, U. T.; Geiger, W. E. *J. Organomet. Chem.* **2001**, *639*, 823−826.
(44) Bildstein, B.; Malaun, M.; Kopacka, H.; Wurst, K.; Ongania, K.-H.; Opromolla, G. *Organometallics* **1999**, *18*, 4325−4336.
(45) Sanders, R.; Mueller-Westerhoff, U. T. *J. Organomet. Chem.* **1996**, *512*, 219−224.
(46) Guillaneux, D.; Kagan, H. B. *J. Org. Chem.* **1995**, *60*, 2502−2505.
(47) Förster, C.; Heinze, K. *Z. Anorg. Allg. Chem.* **2015**, *641*, 517−520.
(48) Siebler, D.; Förster, C.; Heinze, K. *Eur. J. Inorg. Chem.* **2010**, *2010*, 523−527.
(49) (a) Heinze, K.; Siebler, D. *Z. Anorg. Allg. Chem.* **2007**, *633*, 2223−2233. (b) Siebler, D.; Linseis, M.; Gasi, T.; Carrella, L. M.; Winter, R. F.; Förster, C.; Heinze, K. *Chem. - Eur. J.* **2011**, *17*, 4540−4551. (c) Siebler, D.; Förster, C.; Heinze, K. *Dalton Trans.* **2011**, *40*, 3558−3575.
(50) Heinze, K.; Hüttinger, K.; Siebler, D. In *Modeling of Molecular Properties*; Comba, P., Ed.; Wiley-VCH: Weinheim, Germany, 2011.
(51) Kienz, T.; Förster, C.; Heinze, K. *Organometallics* **2014**, *33*, 4803−4812.
(52) Eaton, G. R.; Eaton, S. S.; Barr, D. P.; Weber, Ralph, T. *Quantitative EPR*; Springer: Wien, NY, 2010.
(53) Dempsey, J. L.; Winkler, J. R.; Gray, H. B. *Chem. Rev.* **2010**, *110*, 7024−7039.
(54) Hammes-Schiffer, S. *Chem. Rev.* **2010**, *110*, 6937−6938.
(55) Hammes-Schiffer, S.; Stuchebrukhov, A. *Chem. Rev.* **2010**, *110*, 6939−6960.
(56) Wenger, O. S. *Chem. - Eur. J.* **2011**, *17*, 11692−11702.
(57) Herzog, W.; Bronner, C.; Löffler, S.; He, B.; Kratzert, D.; Stalke, D.; Hauser, A.; Wenger, O. S. *ChemPhysChem* **2013**, *14*, 1168−1176.
(58) Warren, J. J.; Tronic, T. A.; Mayer, J. M. *Chem. Rev.* **2010**, *110*, 6961−7001.
(59) Weinberg, D. R.; Gagliardi, C. J.; Hull, J. F.; Murphy, C. F.; Kent, C. A.; Westlake, B. C.; Paul, A.; Ess, D. H.; Mccafferty, D. G.; Meyer, T. J. *Chem. Rev.* **2012**, *112*, 4016−4093.
(60) Bonin, J.; Robert, M. *Photochem. Photobiol.* **2011**, *87*, 1190−1203.
(61) Savéant, J.-M. *Energy Environ. Sci.* **2012**, *5*, 7718−7731.
(62) Gagliardi, C. J.; Vannucci, A. K.; Concepcion, J. J.; Chen, Z.; Meyer, T. J. *Energy Environ. Sci.* **2012**, *5*, 7704−7717.
(63) Hammarström, L.; Styring, S. *Energy Environ. Sci.* **2011**, *4*, 2379−2388.
(64) Costentin, C.; Robert, M.; Savéant, J.-M. *Phys. Chem. Chem. Phys.* **2010**, *12*, 11179−11190.
(65) Heinze, K.; Schlenker, M. *Eur. J. Inorg. Chem.* **2004**, *2004*, 2974−2988.
(66) Stoll, S.; Schweiger, A. *J. Magn. Reson.* **2006**, *178*, 42−55.
(67) Neese, F. *Wiley Interdiscip. Rev. Comput. Mol. Sci.* **2012**, *2*, 73−78.
(68) Schäfer, A.; Horn, H.; Ahlrichs, R. *J. Chem. Phys.* **1992**, *97*, 2571−2577.
(69) Weigend, F.; Ahlrichs, R. *Phys. Chem. Chem. Phys.* **2005**, *7*, 3297−3305.

DOI: 10.1021/acs.organomet.5b00778
Organometallics 2015, 34, 5310−5320

(70) Neese, F. *Chem. Phys. Lett.* **2000**, *325*, 93−98.
(71) Fischer, T. H.; Almlof, J. *J. Phys. Chem.* **1992**, *96*, 9768−9774.
(72) van Lenthe, E.; Baerends, E. J.; Snijders, J. G. *J. Chem. Phys.* **1993**, *99*, 4597−4610.
(73) Van Wüllen, C. *J. Chem. Phys.* **1998**, *109*, 392.
(74) Pantazis, D. A.; Chen, X. Y.; Landis, C. R.; Neese, F. *J. Chem. Theory Comput.* **2008**, *4*, 908−919.
(75) Sinnecker, S.; Rajendran, A.; Klamt, A.; Diedenhofen, M.; Neese, F. *J. Phys. Chem. A* **2006**, *110*, 2235−2245.

DOI: 10.1021/acs.organomet.5b00778
Organometallics 2015, 34, 5310−5320